Quantifying nanoscale order in amorphous materials: simulating fluctuation electron microscopy of amorphous silicon

2007 J. Phys.: Condens. Matter 19 455204

(http://iopscience.iop.org/0953-8984/19/45/455204)

IOP PUBLISHING JOURNAL OF PHYSICS: CONDENSED MATTER

J. Phys.: Condens. Matter **19** (2007) 455204 (12pp) doi:10.1088/0953-8984/19/45/455204

Quantifying nanoscale order in amorphous materials: simulating fluctuation electron microscopy of amorphous silicon

Stephanie N Bogle[1], Paul M Voyles[2], Sanjay V Khare[1,3] and John R Abelson[2,4]

[1] Department of Materials Science and Engineering and the Materials Research Laboratory, University of Illinois at Urbana-Champaign, Urbana, IL, USA
[2] Department of Materials Science and Engineering, University of Wisconsin-Madison, Madison, WI, USA

E-mail: abelson@mrl.uiuc.edu

Received 28 August 2007
Published 24 October 2007
Online at stacks.iop.org/JPhysCM/19/455204

Abstract

Fluctuation electron microscopy (FEM) is explicitly sensitive to 3- and 4-body atomic correlation functions in amorphous materials; this is sufficient to establish the existence of structural order on the nanoscale, even when the radial distribution function extracted from diffraction data appears entirely amorphous. However, it remains a formidable challenge to invert the FEM data into a quantitative model of the structure. Here, we quantify the FEM method for a-Si by forward simulating the FEM data from a family of high quality atomistic models. Using a modified WWW method, we construct computational models that contain 10–40 vol% of topologically crystalline grains, 1–3 nm in diameter, in an amorphous matrix and calculate the FEM signal, which consists of the statistical variance $V(\mathbf{k})$ of the dark-field image as a function of scattering vector $\mathbf{k}$. We show that $V(\mathbf{k})$ is a complex function of the size and volume fraction of the ordered regions present in the amorphous matrix. However, the *ratio* of the variance peaks as a function of $\mathbf{k}$ affords the size of the ordered regions; and the *magnitude* of the variance affords a semi-quantitative measure of the volume fraction. We have also compared models that contain various amounts of strain in the ordered regions. This analysis shows that the amount of strain in realistic models is sufficient to mute variance peaks at high $\mathbf{k}$. We conclude with a comparison between the model results and experimental data.

[3] Present address: Department of Physics and Astronomy, University of Toledo, Toledo, OH, USA.
[4] Address for correspondence: Department of Materials Science and Engineering, 1-109 Engineering Science Building, MC 233, 1101 W Springfield Avenue, Urbana, IL 61801, USA.

0953-8984/07/455204+12$30.00

1. Introduction

Zachariasen proposed the continuous random network model in 1932 for the structure of amorphous solids; it was subsequently demonstrated to match experimental diffraction data and accepted as good description of the structure [1–3]. However, the lack of techniques available to quantify order on the 1–3 nm length scale has left open the question of whether medium-range order (MRO) also exists in amorphous solids. Elliot defines MRO in covalent amorphous solids (like those considered in this work) as the type of connection (corner-, edge-, or face-sharing) between the coordination polyhedra [4]. The connection between neighboring tetrahedral groups is specified by the dihedral angle, i.e. the relative rotation around a common bond between neighboring tetrahedra. The dihedral angle is random in a CRN, but is precisely 60° in a perfect crystal [4]. Diffraction measurements yield only the two-body correlation function $g(r)$, yielding no evidence of MRO (figure 1) even from atomistic models that are heavily seeded with nanocrystallites (described below). Fluctuation electron microscopy (FEM) [5], however, has been shown analytically to be sensitive to three- and four-body atomic correlations [5–7]. When two pairs of atoms belong to neighboring tetrahedra, then the corresponding four-body function largely reflects the dihedral angle, i.e. whether the structure is locally a CRN or crystalline.

These fluctuations are measured in TEM dark-field images by computing the normalized variance of the diffracted intensity:

$$V(\mathbf{k}, Q)\frac{\langle I^2(\mathbf{r}, \mathbf{k}, Q)\rangle}{\langle I(\mathbf{r}, \mathbf{k}, Q)\rangle^2} - 1 \tag{1}$$

where $\mathbf{r}$ is the position on two-dimensional image, $\mathbf{k}$ is the scattering vector and Q is the radius of the aperture in diffraction space, giving a spatial resolution of $0.61/Q$. As discussed below, given a model of the atomic coordinates, the variance can be calculated either via a direct summation, which is computationally reasonable only for models of ∼60 atoms or less or, as discussed below, by simulating the scattered intensities in the image plane and analyzing these data in the same manner as the experimental data.

FEM has been used to study the existence of MRO in amorphous silicon (a-Si) [8, 9], hydrogenated amorphous silicon (a-Si:H) [10], amorphous germanium (a-Ge) [11], a-Si made by ion implantation, phase-change chalcogenides [12] and amorphous metals [13, 14]. The striking result of FEM studies is that all experimental samples of a-Ge, a-Si, and a-Si:H exhibit peaks in the $V(\mathbf{k})$ function that are inconsistent with the predictions of a CRN model, which exhibits peaks that are only marginally above the background noise.

The ongoing issue is, what structure (or range of structures) is consistent with the electronic and optical properties of these materials AND also predicts the $V(\mathbf{k})$ features? It remains a formidable challenge in diffraction theory to directly invert the FEM data into a detailed atomistic model of the structure. A powerful new method, experimentally constrained molecular relaxation, has been developed to generate structures *a priori* that are consistent with multiple data sets, which may include $V(\mathbf{k})$ [15]. As reported in this workshop [16], the initial results are very promising, but the method has not yet been extensively exploited for a-Si and related materials.

The radial distribution function extracted from diffraction measurements reveals that tetrahedral short-range order is strongly preserved in covalent amorphous materials. One hypothesis is that regions of MRO consist of topologically crystalline (diamond cubic) grains embedded in a CRN matrix. This is plausible considering that it is experimentally straightforward to prepare fine-grained nanocrystalline silicon (having grain sizes of $\geqslant$5 nm) as well as mixed-phase samples. Previous authors have called such models 'paracrystalline Si' and showed that they produce simulated $V(\mathbf{k})$ peaks at the same positions as those observed

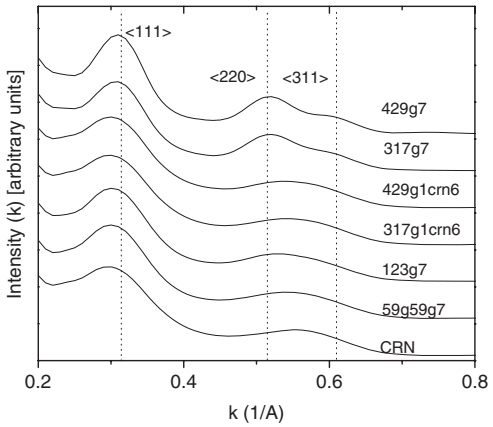

Figure 1. Average scattered intensities for various models, arbitrary offset in magnitude.

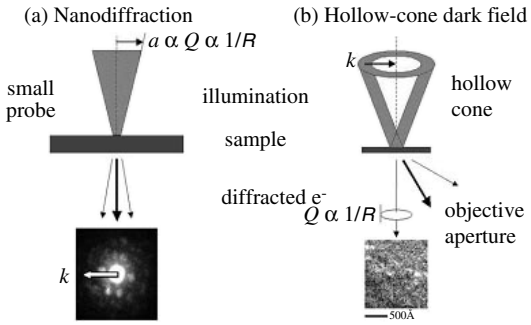

Figure 2. Two modes: (a) variable resolution FEM via nanodiffraction and (b) variable coherence FEM via HCDF.

experimentally [17, 18]. In this work, we obtain quantitative interpretations using a forward modeling approach. We generate a family of paracrystalline silicon models that contain varying amounts of order, simulate the FEM data from these models, extract trends as a function of the size and volume fraction of the ordered regions, and compare these simulations with experimental data.

2. Implementation on the TEM

Experimentally, FEM data can be collected using two different methods: hollow cone dark field (HCDF) TEM and nanodiffraction in the STEM (figure 2). In HCDF, the FEM signal is generated by taking a series of dark-field TEM images at several different areas of a sample, calculating the variance in each image, and averaging the resulting variances. In STEM–FEM, nanodiffraction patterns are collected across a region of the sample. The intensity in the patterns is rotationally averaged and the variance from image to image is calculated. These two methods collect the same data set, by the principle of optical reciprocity. The HCDF mode is accessible on traditional TEMs, but it does not easily permit changes in resolution. Gibson *et al* have shown that the characteristic length of the MRO, defined as the point at which the correlation between atom pairs typically decays, can be extracted from $V(Q)$ at constant $\mathbf{k}$ [7]. In STEM,

variable resolution is more easily performed: multiple probe size can be obtained from the same aperture simply by adjusting the excitation of a condenser lens between the physical aperture and the objective lens [19, 20].

In addition, STEM allows for easy identification of regions with unusually large ($\geqslant$4 nm) nanocrystalline features that will dominate the variance signature [21]. The major influence of a nanoparticle can be understood as follows: the scattered intensity I from an isolated crystal increases as N^2, where N is the number of atoms, and therefore as the radius R^6; although this intensity is folded into the overall variance (equation (1)), the R^6 dependence gives a huge weighting factor to larger crystallites. These regions can, if desired, be filtered out in STEM by identifying the corresponding nanodiffraction patterns and removing them from the data set, allowing for computation of the variance in the majority of the film. Note that FEM theories developed thus far assume fully coherent imaging conditions, which maximizes the variance. Measurements carried out in a STEM approach this condition, and thus the magnitude of the variance found experimentally can be compared with that predicted in the present simulations. By contrast, the coherence in a conventional TEM is smaller, and thus the experimental data will exhibit smaller absolute magnitude, by a factor that ranges from 2 to 10 depending on the instrument, as discussed elsewhere in this volume [22].

3. Model development

A realistic structural model of a-Si must reproduce, via accurate simulations, the electronic, vibrational and optical properties that are measured experimentally. As noted by Drabold [23], no computational algorithm exists that can reproduce the *actual* pathway by which a real material is synthesized, as all algorithms that involve physical atom trajectories involve unphysical timescales. For example, molecular dynamics 'quench from the melt' techniques can only be performed for extremely short equivalent times ($<$1 ns), which implies extreme cooling rates. The resulting models contain a significant fraction of 3- and 5-fold coordinated Si atoms that create a huge density of states within the mobility gap, i.e. the electronic properties are unrealistic [24]. To generate a high quality model, the algorithm must intrinsically incorporate the physical features that are known to exist. The Wooten, Weiner, and Weaire (WWW) method [25] assumes that four-fold (tetrahedral) coordination is the key feature, and maintains it as follows. Atoms are placed randomly inside a computational box, assigned four neighbors, and then allowed to relax through bond-switching events (bonds A–B and C–D become bonds A–C and B–D) when such switches reduce the total energy. Local structural rearrangements follow bond-switching transpositions. This process is continued until the system reaches a local deep minimum, i.e. the lowest energy state while remaining amorphous. CRN structures synthesized using WWW are highly realistic in terms of bond angle and bond length distributions, total energy, electronic and vibrational properties [26]. Molecular dynamics simulations suggest that the structural relaxation of a-Si in fact occurs via bond-switching events, which may explain the success of the WWW approach [26].

Nakhmanson *et al* extended the WWW approach to the synthesis of paracrystalline silicon and showed that the resulting model predicts the measured electronic and vibrational properties of a-Si [24] and yields peaks in the variance function $V(\mathbf{k})$ at the $\mathbf{k}$ vectors that are observed experimentally [24]. However, only a few models were synthesized, such that detailed trends could not be extracted. We employ the same algorithm to create a family of models that spans a broad range of paracrystallite grain sizes and volume fractions (figure 3). First, one to four spherical grains of crystalline silicon are positioned inside of an empty computational cell that will ultimately contain 1000 atoms. The number and size of grains specifies, by construction, the volume fraction of the atoms that have a locally crystalline environment. The grains are

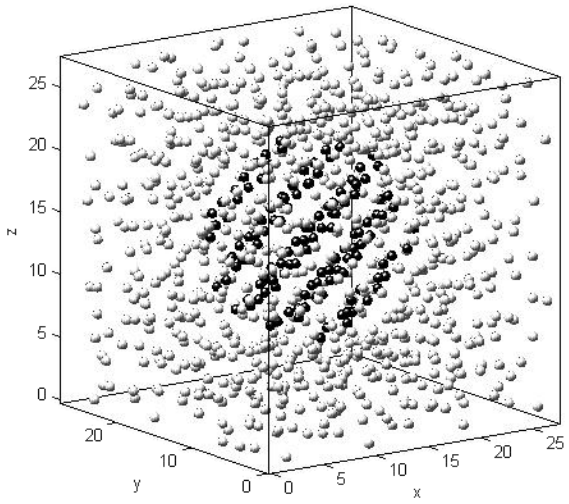

Figure 3. A paracrystalline cell with 1 paracrystal of 123 atoms, surrounded by a CRN matrix.

each rotated to a random orientation and the remaining volume is randomly filled with atoms. All of the atoms in the cell are assigned bonds with 4 neighbors. Next, the system is allowed to relax via bond-switching except for atoms that are completely within the grains, the so-called paracrystallites, whose coordinates are fixed. After the energy of the system is significantly minimized, the atoms in the grains are allowed to move to obtain a final energy minimization. To test whether the resulting models are physically reasonable, Drabold *et al* input the atomic coordinates from selected WWW paracrystalline models into a first-principles code and then allowed the system to relax. Negligible changes occurred in the coordinates, confirming the quality of the WWW synthesis method [27].

It is known experimentally that peaks in both the scattered *intensity* and in the FEM *variance* for a-Si occur at **k** vectors similar to those for Bragg diffraction in crystalline silicon from the ⟨111⟩, ⟨220⟩, and ⟨311⟩ planes. These peak positions (referred to throughout as the 1st, 2nd, and 3rd peaks, respectively) and peak widths are reproduced by the WWW paracrystalline models. Because the peak widths are nearly constant, the interpretation of FEM spectra involves only the heights of the characteristic peaks. For a CRN model with no paracrystallites, the intensity shows similar peaks, as expected due to the tetrahedral short-range order (figure 1), but the FEM variance has a low magnitude (figure 4). For models that have large paracrystalline content, the variance peaks due to the CRN are negligible; however, the non-zero CRN background sets a modest lower limit on the ability of FEM to detect dilute paracrystalline content.

To study the effect of paracrystalline size and volume fraction on the FEM variance, we constructed thirteen computational cells of 1000 atoms each, 2.7 nm on a side, using the WWW method (table 1). For each cell, the designation code (number g) gives the number of atoms in each paracrystalline grain; cells containing two or four grains have two or four codes. The grain sizes range from 1.10 to 2.54 nm in diameter and the ordered volume fractions range from 12 to 40%. All of these cells have roughly Gaussian distributions of bond angles, $109° \pm 10°$, and of bond lengths, 2.35 ± 0.1 Å, values which are characteristic of the best a-Si models. In order to reproduce the film thickness used in experiment (∼20 nm), seven cells are stacked in the z-direction (parallel to the electron beam in the TEM) to give a total simulated thickness of ∼19 nm. Voyles has shown [6] that variance data must be corrected for film thickness;

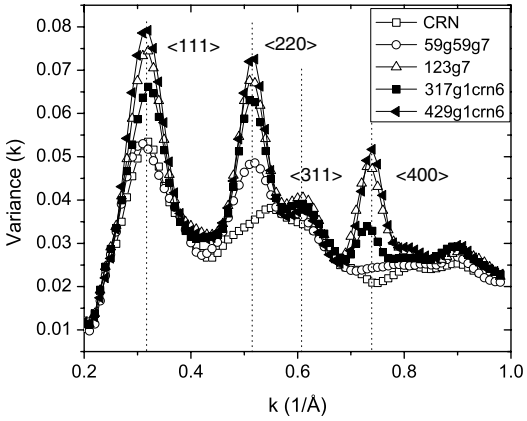

Figure 4. Variance calculated for a continuous random network (open squares) and various Si models with low paracrystalline fraction.

Table 1. Nomenclature of paracrystalline silicon cells. Each cell contains 1000 atoms. The models are named by the number of atoms per grain, for each of the grains in the computational cell.

Model name	# Grains	Largest diameter (nm)	Volume% crystalline
123g	1	1.68	12
211g	1	2	21
317g	1	2.3	32
429g	1	2.54	43
123g87g	2	1.68	21
163g163g	2	1.84	32
211g211g	2	2	42
59g59g	2	1.31	12
163g123g87g59g	4	1.84	43
163g59g59g35g	4	1.84	32
35g35g35g35g	4	1.1	12
59g59g59g59g	4	1.31	21
crn1000	0	0	0

however, only a weak dependence is shown between thicknesses of 10–22 nm in a-Si. Prior to stacking, the individual cells are randomly rotated and randomly translated in the x and y directions, but without creating any void spaces. The use of a random rotation creates a statistically isotropic material. Selected simulations combine different computational cells in the same stack, e.g. to investigate the effect of introducing a paracrystallite size distributions or of diluting the paracrystalline cells with cells of CRN. The designation code for the stacked model now gives the number of each type of cell after the number g, e.g. 317g1crn6 indicates a model containing 1 cell of 317g and 6 cells of CRN. To obtain good sampling statistics, $I(\mathbf{r}, \mathbf{k})$ is calculated from 200 equivalent stacks, where the component cells are randomly rotated and shifted in *each* of the 200 stacks. For 1.1 nm instrument resolution, this gives a total of greater than 5000 pixels in the simulated dark-field image, resulting in an observed sampling induced error of less than 1% in the calculated $V(\mathbf{k})$. At the boundaries between computational cells the atomic positions are random. This is unphysical (tetrahedral short-range order should be preserved), but the number of atoms in the cell boundaries is a small fraction of the total. To

check that boundary effects are negligible, we introduced extra boundaries into several test stacks and found no difference in the simulated $V(\mathbf{k})$ spectra.

We also investigated the possible role of strain on the $V(\mathbf{k})$ data. As described above, the synthesis of the paracrystalline models allows the atoms within the grains to adjust their positions in order to minimize the system energy. To construct a strain-free analogue, we first created several cells in which spheres of perfect crystalline Si are suspended in space; each of these has the same number and size of grains as in one of the paracrystalline models. We then stacked one or more of these cells together with cells of CRN to achieve nearly the same number of atoms per unit area, as projected through the total thickness, as in the corresponding stacked pc-Si model. Finally we computed the variance for 200 such stacks, introducing random rotations and displacements as before. This approach assumes that the physical separation of the crystalline spheres and the CRN does not introduce significant errors because these atoms are combined in projection; this is borne out by the reasonableness of the results.

We had previously shown that introducing preferred orientation into the paracrystalline models does influence the heights of the variance peaks [17]. In the absence of experimental data that indicate anisotropy, we do not consider that possibility in the present work.

Here, we simulate the dark-field hollow cone image for each stack of computational cells using FEMSIM, which uses an algorithm developed by Keblinski [28]. This code is optimized for the present purposes, i.e., to calculate the intensity scattered by all the atoms within the projected resolution volume on each pixel. While this code can handle any resolution, it is computationally efficient to limit the resolution to two-thirds the width of the model or less. The program currently considers single scattering only. Multiple scattering effects are considered insignificant for a-Si films less than 25 nm in thickness [29]; for heavier atoms, multiple scattering effects would need to be considered, or the thickness should be reduced. The simulations presented here use a constant resolution of 1.1 nm because: (i) smaller resolutions give larger variance signatures; (ii) this resolution is readily available on both our TEM and our STEM; (iii) it is computationally fast; and (iv) our objective to determine what quantitative information can be easily extracted from a single variance curve, which is the most readily available experimental information to users of TEMs.

4. Results and discussion

The paracrystalline silicon model simulations afford $V(\mathbf{k})$ signatures that reveal the separate effects of paracrystallite size versus volume fraction and show that strain effects in the paracrystalline grains are non-negligible. $V(\mathbf{k})$ is a complex and non-linear function of paracrystallite size and volume fraction. When the paracrystal size is held fixed and the volume fraction changed, the *relative* heights of the 1st through 3rd peaks remain constant but the *absolute* magnitude changes (figure 5). When the volume fraction is held constant and the paracrystallite size changed, the peak magnitudes also change. However, for monodisperse models these contributions can be deconvoluted: we have determined that the size of the paracrystalline regions can be extracted, *independent of the volume fraction*, by taking the ratio of the 1st to 2nd peaks (at $k = 0.31$ and 0.53 Å, respectively) and separately the ratio of the 2nd to 3rd peaks (the latter at $k = 0.61$ Å). These peak height ratios vary linearly as a function of paracrystallite diameter (figure 6). The relationship reported in figure 6 holds true for volume fractions greater than ∼3% (this limit is also a function of paracrystallite size). At this volume fraction or smaller, the 3rd peak is no longer distinguishable, and the variance resembles that of a CRN. Once the size of the paracrystallites is known, the magnitude of the 1st peak can be used to estimate the crystalline volume fraction (figure 7). Recall that the absolute height of $V(\mathbf{k})$ also varies with the coherence of the imaging mode; thus data taken on different instruments

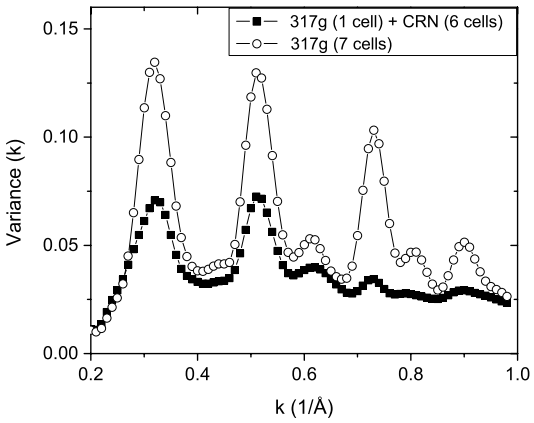

Figure 5. $V(\mathbf{k})$ at 1.1 nm resolution for two different volume fractions of the 317g cells.

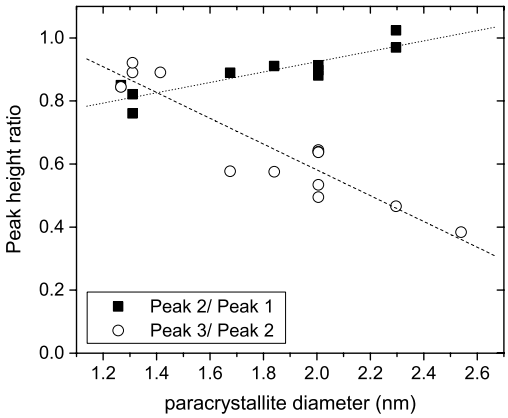

Figure 6. Peak height ratios (peak 2/peak 1 and peak 3/peak 2) at 1.1 nm resolution for monodisperse pc-Si models of various paracrystalline volume fraction as a function of paracrystallite diameter. Dotted lines are linear least square fits to the data.

should not be compared in the absence of calibration data, i.e. samples that have been analyzed on both instruments.

Real systems will have a polydisperse size distribution. Our study shows that for polydisperse systems it is difficult to extract the relative contributions of size versus volume fraction from the $V(\mathbf{k})$ data. However, figure 6 allows us to set some bounds on the overall structure of a mixed system. We stack models of varying paracrystallite size and volume fraction, simulate the variance, and then attempt to interpret the data in terms of paracrystallites size and volume fraction. Here (open circles, figure 8), the distribution of polydisperse model is 1/13 of large (2.5 nm) paracrystals and 12/13 of small (1.3 nm) paracrystals. From the peak height ratio plot, we would (conservatively) estimate a probable size of 1.5–2.2 nm. In the absence of a large peak magnitude, we would also correctly conclude that there are relatively few of the large paracrystallites present. To obtain more detailed information on size distributions, more sophisticated data mining from STEM nanodiffraction patterns and/or more sophisticated theory will be required.

Strain effects are revealed by comparing the paracrystalline models with the models consisting of perfect crystalline spheres combined with the CRN matrix. In the perfect

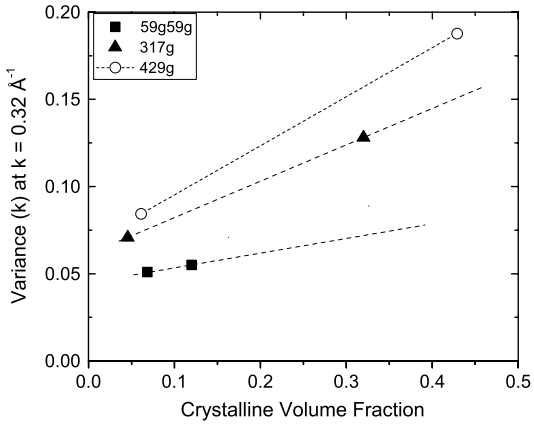

Figure 7. The dotted lines are fits to the magnitude of the peak one versus volume fraction for models containing the same size paracrystallites.

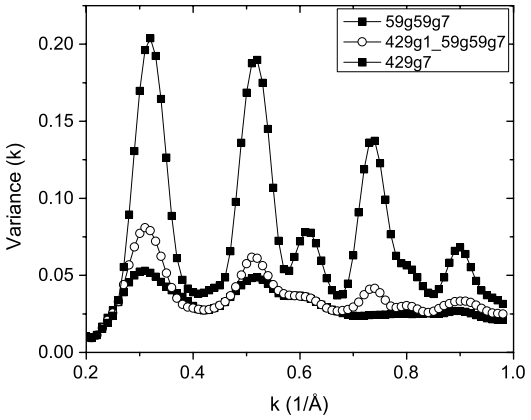

Figure 8. Variance (k) for paracrystalline model 429g(1 cell) + 59g59g(6 cells) in comparison to models 429g7 and 59g59g7.

crystalline model the variance peaks are large at high **k** whereas they are suppressed in the paracrystalline model (figure 9). This indicates that strain fields are very significant in paracrystalline silicon; strain more strongly damps diffraction from closely spaced high-**k** planes, reducing their influence on the variance in paracrystalline versus perfectly shaped crystalline spheres. The muting of the 2nd and 3rd peaks, and the complete absence of the 4th peak, in this case, are consistent with experimental data. Visual inspection of the paracrystalline models reveals significant displacements within the grains, including curvature of atomic planes. Such an effect is not surprising in view of the topological transition between the crystalline and amorphous matrix. For example, in the CRN the bond angle deviation is $\pm 10°$, and since tetrahedral bonding is continuous, we should expect distortions to extend within the grain. Simulations of the electronic structure reveal that the conduction band tail states are localized around the periphery of the grains, which is presumably a strain effect [24].

These results show that strain must be considered when extracting size and volume fraction information from variance peaks. It could be argued that this complication invalidates the relationships shown in figures 6 and 7. We respond as follows. It is widely found that

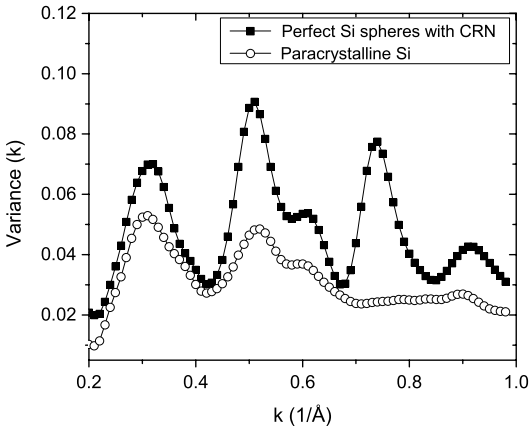

Figure 9. Comparison of simulated $V(\mathbf{k})$ for 59g59g ($d = 1.3$ nm) pc model (open circles) and 1.3 nm crystalline spheres of Si suspended in space in stacks with cells of CRN to achieve equivalent projected atom density (closed circles).

experimental samples of a-Si have nearly the same bond angle and length deviations as found in the present computational models; these facts indicate that the experimental synthesis method, although far from real equilibrium, allows enough relaxation for the sample to develop strain fields that are reproducible and presumably similar to those in the WWW computational cells. Thus the trends shown in figures 6 and 7 should be robust. On the other hand, it may be possible to alter the strain fields by alloying, especially with hydrogen, which inserts into strained Si–Si bonds and decorate the network with Si–H bonds [30, 31]. In a previous experimental study, we introduced atomic hydrogen into an a-Si sample grown at 350 °C, observed that the second peak increased in magnitude, and interpreted that the paracrystalline regions must have increased in size [10]. The results in figure 9 offer an alternative explanation: the introduction of hydrogen may have provided enough relaxation that the strain fields diminished within the grains, thus increasing the variance. To determine which effect is dominant, it will be necessary to acquire variable resolution FEM data using a STEM *and* to determine the extent to which the correlation length extracted from the analysis is influenced by strain.

The present simulations provide the best agreement to date with experimental FEM results (figure 10). In accord with previous FEM studies on magnetron sputtered a-Si grown at various substrate temperatures [9], we find that both the 1st and 2nd peaks increase in intensity as the regions of order (paracrystallites) grow in size, and that the 2nd peak ultimately becomes larger than the 1st. The present work shows that the peak height ratios provide a quantitative measure of the paracrystallite size, independent of the volume fraction. For example, analysis of the aforementioned experimental spectra using the peak ratios (figure 7) indicates that the paracrystallite size increases from 2.4 to 3.7 nm the substrate temperature increases from 200 to 350 °C.

An apparent discrepancy is that the 3rd peak is rarely resolved from the 2nd peak in real experiments, whereas it is clearly visible in most of the simulations. We previously observed the peak splitting in hydrogenated a-Si:H samples when the image area being analyzed contained 1 or 2 very large crystallites (>4 nm) [21]. (The films analyzed in that study were prepared using high-pressure plasma enhanced CVD, in which Si nano-aggregates nucleate in the gas phase and land on the film growth surface.) However, when the data from all the sampled areas were averaged together, the peak splitting could no longer be resolved in $V(\mathbf{k})$. We interpret

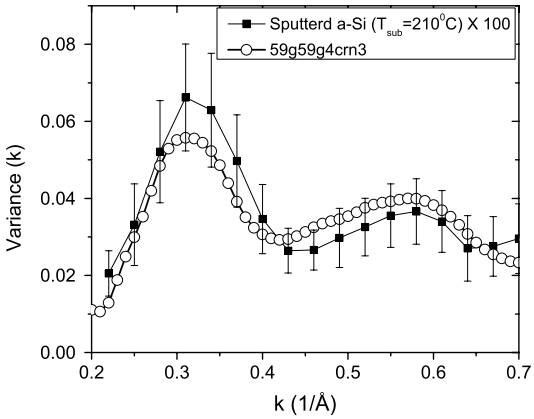

Figure 10. Comparison of $V(\mathbf{k})$ for magnetron sputtered a-Si at a substrate temperature of 210 °C (nominally the same as from [10]) and paracrystalline model 59g59g4crn3.

that most experimental samples do not contain enough large paracrystallites to produce peak splitting. In our simulations, the volume fraction of large crystallites ($>$2 nm) must be $>$1% to resolve the peak splitting or $>$7% for small crystallites ($<$1.5 nm), i.e. the lack of peak splitting serves as an indirect metric of the fraction. In STEM, the peak splitting is more difficult to find because the total area sampled is $\sim$500 nm^2 whereas in HCDF, the area sampled is $\sim$100 000 nm^2. It is also possible that the current models do not capture some structural aspect of the real material; strain is the most likely suspect, although if the real material were more highly strained than the WWW models, then it would be less likely to observe a 2nd peak which is both large in magnitude and also merged (unresolved) with the 3rd peak.

There is also an apparent discrepancy between the continuous increase in variance with volume fraction of ordered regions deduced in this work and the maximum in variance at a volume fraction of 2.5% predicted using the analytical formalism of Stratton and Voyles [32]. The latter authors assumed regions of perfect crystalline silicon in their model and a constant intensity from the CRN, whereas the WWW synthesis routine used in our study allowed strain to occur in the paracrystalline regions and produced a non-zero variance for the CRN. They also assumed an unrealistic sample geometry in which the crystal grains occupy a simple cubic lattice, leading to excessive overlap of the grains in projection. Thus, strain again appears as an important effect that deserves additional consideration in future research. As pointed out by Gibson [33] in his contribution to this volume, strain effects are expected to be large in tetrahedral covalent materials due to the angular nature of bonding, and significantly smaller in materials that lack directional bonding such as amorphous metals.

5. Conclusions

We have quantified the FEM method for a-Si by forward simulating the FEM data from a family of paracrystalline silicon models. The resulting models give the best fit to experimental FEM to date. The FEM signal generated from these models show that $V(\mathbf{k})$ is a complex function of size and volume fraction of the ordered regions present in the amorphous matrix. However, the ratio of the variance peaks as a function of $\mathbf{k}$ affords the size of the ordered regions, and the magnitude of the variance affords a semi-quantitative measure of the volume fraction. We have also shown that variance from experimental films contain strain. Thus, strain must be considered when extracting size and volume fraction information from variance peaks.

Acknowledgments

We are grateful to the National Science Foundation for support of this work under grants DMR 02-05858 and DMR 06-05890. SNB also acknowledges the International Materials Institute-New Functionality in Glass Scholarship for travel support to the International Workshop on Nanoscale Order in Amorphous and Partially Ordered Solids (Cambridge UK, 9–11 July 2007), for which this paper was written. We thank David A Drabold, Ohio University, for many useful suggestions.

References

[1] Zachariasen W H 1932 *J. Am. Chem. Soc.* **54** 3841
[2] Polk D E 1971 *J. Non-Cryst. Solids* **5** 365
[3] Polk D E and Boudreaux D S 1973 *Phys. Rev. Lett.* **31** 92
[4] Elliott S R 1991 *Nature* **354** 445
[5] Treacy M M J and Gibson J M 1996 *Acta Crystallogr.* A **52** 212–20
[6] Voyles P M 2001 *Thesis* University of Illinois at Urbana-Champagin
[7] Gibson J M, Treacy M M J and Voyles P M 2000 *Ultramicroscopy* **83** 169–78
[8] Treacy M M J, Gibson J M and Keblinski P J 1998 *J. Non-Cryst. Solids* **231** 99–110
[9] Voyles P M, Gerbi J E, Treacy M M J, Gibson J M and Abelson J R 2001 *Phys. Rev. Lett.* **86** 5514
[10] Nittala L N, Jayaraman S, Sperling B A and Abelson J R 2005 *Appl. Phys. Lett.* **87** 241915
[11] Gibson J M and Treacy M M J 1997 *Phys. Rev. Lett.* **78** 1074
[12] Kwon M H, Lee B S, Bogle S N, Nittala L N, Abelson J R, Bishop S G, Raoux S, Cheong B K and Kim K B 2007 *Appl. Phys. Lett.* **90** 021923
[13] Stratton W G, Hamann J, Perepezko J H, Voyles P M, Mao X and Khare S V 2005 *Appl. Phys. Lett.* **86** 141910
[14] Stratton W G, Hamann J, Perepezko J H and Voyles P M 2006 *Intermetallics* **14** 1061
[15] Biswas P, Tafen D and Drabold D A 2005 *Phys. Rev.* B **71** 054204
[16] Biswas P, Atta-Fynn R and Drabold D A 2007 *J. Phys.: Condens. Matter* **19** 455202
[17] Khare S V, Nakhmanson S M, Voyles P M, Keblinski P and Abelson J R 2004 *Appl. Phys. Lett.* **85** 745
[18] Voyles P M, Zotov N, Nakhmanson S M, Drabold D A, Gibson J M, Treacy M M J and Keblinski P 2001 *J. Appl. Phys.* **90** 4437
[19] Voyles P M and Muller D A 2002 *Ultramicroscopy* **93** 147–59
[20] Nittala L N, Bogle S N, Tweston R D, Voyles P M and Abelson J R 2007 unpublished
[21] Nguyen-Tran T, Nittala L N, Bogle S N, Suendo V, Rocca i Cabarrocas P and Abelson J R 2006 *J. Appl. Phys.* **100** 094319
[22] Stratton W G and Voyles P M 2007 *J. Phys.: Condens. Matter* **19** 455203
[23] Drabold D A and Li J 2001 *Curr. Opin. Solid State Mater. Sci.* **5** 509
[24] Nakhmanson S M, Voyles P M, Mousseau N, Barkema G T and Drabold D A 2001 *Phys. Rev.* B **63** 235207
[25] Wooten F, Winer K and Weaire D 1985 *Phys. Rev. Lett.* **54** 1392
[26] Mousseau N and Barkema G T 2000 *Phys. Rev.* B **61** 1898
[27] Chakraborty S and Drabold D A 2007 at press
[28] Dash R K, Voyles P M, Gibson J M, Treacy M M J and Keblinski P 2003 *J. Phys.: Condens. Matter* **15** S2425
[29] Treacy M M J and Gibson J M 1993 *Ultramicroscopy* **52** 31
[30] Jackson W B and Tsai C C 1992 *Phys. Rev.* B **45** 6564
[31] von Keudell A and Abelson J R 1997 *Appl. Phys. Lett.* **26** 3832
[32] Stratton W G and Voyles P M 2007 *Ultramicroscopy* submitted
[33] Gibson J M 2007 *J. Phys.: Condens. Matter* **19** 455217